Available online at www.sciencedirect.com

ScienceDirect

Biomedical Journal

journal homepage: www.elsevier.com/locate/bj

Original Article

Organ defects of the *Usp7*^{K444R} mutant mouse strain indicate the essential role of K63-polyubiquitinated Usp7 in organ formation

Han-Tsang Wu [a,1], *Yueh-Te Lin* [b,1], *Shan Hwu Chew* [c], *Kou-Juey Wu* [b,d,e,*]

[a] *Department of Cell and Tissue Engineering, Changhua Christian Hospital, Changhua, Taiwan*
[b] *Cancer Genome Research Center, Chang Gung Memorial Hospital at Linkou, Taoyuan, Taiwan*
[c] *Cancer Research Malaysia, Outpatient Centre, Sime Darby Medical Centre, Subang Jaya, Selangor, Malaysia*
[d] *Institute of Cellular and Organismic Biology, Academia Sinica, Taipei, Taiwan*
[e] *Inst. of Clinical Medical Sciences, Chang Gung University, Taoyuan, Taiwan*

ARTICLE INFO

Article history:
Received 6 October 2021
Accepted 9 February 2022
Available online 18 February 2022

Keywords:
Usp7
K63-linked polyubiquitination
Knock-in mouse
Glycogen storage
Polycystic kidney

ABSTRACT

Background: K63-linked polyubiquitination of proteins have nonproteolytic functions and regulate the activity of many signal transduction pathways. USP7, a HIF1α deubiquitinase, undergoes K63-linked polyubiquitination under hypoxia. K63-polyubiquitinated USP7 serves as a scaffold to anchor HIF1α, CREBBP, the mediator complex, and the super elongation complex to enhance HIF1α-induced gene transcription. However, the physiological role of K63-polyubiquitinated USP7 remains unknown.

Methods: Using a *Usp7*^{K444R} point mutation knock-in mouse strain, we performed immunohistochemistry and standard molecular biological methods to examine the organ defects of liver and kidney in this knock-in mouse strain. Mechanistic studies were performed by using deubiquitination, immunoprecipitation, and quantitative immunoprecipitations (qChIP) assays.

Results: We observed multiple organ defects, including decreased liver and muscle weight, decreased tibia/fibula length, liver glycogen storage defect, and polycystic kidneys. The underlying mechanisms include the regulation of protein stability and/or modulation of transcriptional activation of several key factors, leading to decreased protein levels of Prr5l, Hnf4α, Cebpα, and Hnf1β. Repression of these crucial factors leads to the organ defects described above.

Conclusions: K63-polyubiquitinated Usp7 plays an essential role in the development of multiple organs and illustrates the importance of the process of K63-linked polyubiquitination in regulating critical protein functions.

* *Corresponding author*. Cancer Genome Research Center, Chang Gung Memorial Hospital at Linkou, 5, Fusing St., Gueishan, Taoyuan 333, Taiwan.
E-mail address: wukj@cgmh.org.tw (K.-J. Wu).
Peer review under responsibility of Chang Gung University.
[1] These authors contributed equally to this work.
https://doi.org/10.1016/j.bj.2022.02.002

At a glance commentary

Scientific background on the subject

K63-linked polyubiquitination of proteins have non-proteolytic functions and regulate the activity of many signal transduction pathways. USP7, a HIF1α deubiquitinase, undergoes K63-linked polyubiquitination under hypoxia, serving as a scaffold to anchor HIF1α-associated transcription complex to enhance gene transcription. However, the physiological role of K63-polyubiquitinated USP7 in organ development remains unknown.

What this study adds to the field

Multiple organ defects, including decreased liver and muscle weight, decreased tibia/fibula length, liver glycogen storage defect, and polycystic kidneys are observed in *Usp7*^{K444R} point mutation knock-in mice. Therefore, K63-polyubiquitinated Usp7 plays an essential role in organ development and illustrates the importance of K63-linked polyubiquitination in regulating critical protein functions.

Lysine-63 (K63)-linked polyubiquitination of proteins has non-proteolytic functions, including protein trafficking, NF-kB activation, DNA damage repair, kinase and phosphatase activation, chromatin dynamics [1–11]. Among these examples, activation of the NF-kB pathway has been shown to require K63-linked polyubiquitination [4–6]. Other signal transduction molecules, including AKT1, IRF1, RIG-1, Toll-like receptor, T-cell receptor, NOD-like receptor, have also been shown to undergo K63 polyubiquitination to carry out their functions [7–10]. One of the functions of K63-linked polyubiquitin chains is to serve as a scaffold to facilitate the assembly of a protein complex [11].

Deubiquitinases are known to exhibit multiple functions [12–15]. One of the best characterized deubiquitinases, USP7 (HAUSP), is a USP-type deubiquitinase that deubiquitinates different substrates, including TP53, MDM2, REST, PTEN, HIF1α and other proteins, to increase their stability [16–25]. In terms of biological functions, USP7 stabilizes MDM2 and other substrates to mediate their oncogenic functions [21]. Numerous results have indicated that USP7 plays a crucial role in tumorigenesis [16–18,21,22,24,25]. Regarding development, *Usp7*-null mice are embryonic lethal [26]. Neuronal *Usp7*-null mice demonstrate neonatal lethality and brain hypoplasia [27]. However, the specific functions of USP7 in organ formation are very difficult to assess since even neuron-specific *Usp7*-knockout mouse strains exhibit early lethality, and the effects of Usp7 on organ formation in the later stage of mouse development cannot be elucidated [26,27]. Generating a hypomorphic *Usp7* mutant mouse strain may be another way to evaluate the function of Usp7 in a living animal. We previously demonstrated that mutation of the K63 polyubiquitination site (K443) of USP7 significantly decreases the ability of USP7 to stabilize HIF1α under hypoxia due to its impaired deubiquitinase activity [25]. In addition, this USP7 point mutant is also impaired in its ability to serve as a scaffold to anchor HIF1α, CREBBP, the mediator complex, and the super elongation complex to enhance hypoxia-induced gene transcription [25]. Therefore, the *Usp7*^{K444R} knock-in mutant mouse strain may serve as a *Usp7* hypomorphic strain that can allow us to assess the physiological functions of Usp7 in mice.

One of the major factors controlling organ size is the cell growth rate, which is regulated by the rates of cell cycle progression and cell proliferation [28]. The mTORC2 complex-regulated signaling has been shown to be a crucial pathway to regulate cell proliferation [29]. The mTORC2 complex is composed of MTOR, RICTOR, DEPTOR, MAPKAP1, and PRR5/PRR5L [29–32]. The mTORC2 complex mainly regulates AKT1 phosphorylation (at the Ser-473 site) to control cell proliferation and cell size [29–31]. Whether any of the components within the mTORC2 complex is a substrate of USP7 remains unknown. The Hippo pathway is a major regulator of organize size through YAP/TAZ [33]. YAP is a substrate of USP7 [34], implicating USP7 in organ size control. YAP can also be regulated by the FGF15-MST1/2 signaling and MST1/2-YAP pathway plays a role in liver overgrowth and tumorigenesis [35,36]. Whether the FGF15-MST1/2 signaling is involved in USP7-regulated cell growth remains to be determined.

Liver glycogen storage is important for liver function, and glycogen is synthesized by glycogen synthase 2 (GYS2) [37]. *GYS2* expression is regulated by HNF4α and CEBPα [38–40]. Polycystic kidney disease (PKD) is an important human disease that may be autosomal dominant or recessive [41–43]. PKD is primarily caused by mutations in the *PKD1* and *PKD2* genes [41–43]. Because *Pkd2* and *Pkd1* expression is regulated by Hnf1β, renal-specific inactivation of Hnf1β in mice causes PKD [44]. Although mutations of *GYS2* or *PKD1/2* genes may cause glycogen storage defect or PKD, other non-mutational mechanisms that regulate the expression or function of these genes remain to be determined.

In this report, we show that *Usp7*^{K444R} knock-in mutant mouse exhibit organ defects including decreased liver and muscle weight, decreased tibia/ulna length, deficient liver glycogen storage, and PKD. Various signaling pathways are affected by the *Usp7*^{K444R} mutation in these mice. These results demonstrate the essential role of K63-linked polyubiquitinated Usp7 in carrying out crucial functions during the formation of certain vital organs.

Materials and methods

Animals and tissue preparation

The homozygous *Usp7*^{K444R} mutant (corresponding to K443R mutation in USP7) mouse strain was generated as described [25]. All organs were obtained after mouse heart perfusion by saline and fixed by 4% paraformaldehyde solution for 24 h for H&E and IHC, or immediately homogenized in T-PER™ Tissue Protein Extract Reagent (Thermo Fisher Scientific Inc., USA) by tissue homogenizer (HT mini homogenizer, OPS Diagnostics

LLC, USA) for Western blot analysis. Handling of the animals has been approved by the Internal Animal Usage Committee of the Chang Gung Memorial Hospital at Linkou.

Cell culture

The NeHepLxHT (neonatal human normal hepatocyte) cell line was obtained from ATCC (American type culture collection), and the embryonic kidney 293T cell line was described [25]. Culture conditions of the cell lines were described [25]. Screening of Mycoplasma contamination was negative for these cell lines.

Protein extraction, Western blot analysis, RNA extraction, and quantitative real-time PCR

M-PER™ mammalian protein extract reagent (Thermo Fisher Scientific Inc., USA) was used for extraction of protein from all cells as described [25]. Protein concentration determination and Western blot analysis were described [25]. The characteristics of the antibodies used were listed (Table S1). RNA purification, cDNA synthesis and quantitative real-time PCR (qPCR) analysis were performed as described [25]. The sequences of primers used in the real-time PCR experiments were shown (Table S2).

Deubiquitination assay

For deubiquitination assay, Flag-USP7 wild type and its mutants were respectively overexpressed in 293T cells, immunoprecipitated by anti-Flag agarose (Sigma), and eluted by Flag peptides (100 μg/mL) in the deubiquitination buffer (50 mM Tris–HCl pH 8.0, 50 mM NaCl, 1 mM EDTA, 10 mM DTT, 5% glycerol). The poly-Ub-Myc-PRR5L were expressed in 293T cells by transient transfection with Myc-tag-PRR5L and ubiquitin plasmids under MG132 treatment, precipitated by anti-Myc beads (Sigma). Purified poly-Ub-Myc-PRR5L, Flag-USP7 and its mutants were incubated in a deubiquitination buffer for 15–30 min at 37 °C and subjected to Western blot analysis.

Immunoprecipitation and qChIP analysis

Immunoprecipitation was performed as described [25]. For qChIP assays, tissues were homogenized after perfusion with saline and cross-linked with 1% formaldehyde for 10 min, and stopped by adding glycine to a final concentration of 0.125 M. Fixed cells or tissues were washed twice with Tris-buffered saline (20 mM Tris, pH 7.5, and 150 mM NaCl) and harvested in 2 mL PBS buffer with protease inhibitors. DNA fragment extraction from beads was performed using the Chromatin Immunoprecipitation (ChIP) assay kit (Merck Millipore, Billerica, MA, USA). For analysis of qChIP products, DNA samples were quantified by the SYBR Green assay using 1× SYBR Green Mixture (Kapa Biosystems, Woburn, MA, USA) with specific primers in a total volume of 20 μL. Data were analyzed by the CT method and plotted as % input DNA. qChIP values were calculated by the following formula: % input recovery = [100/(input fold dilution/bound fold dilution)] × $2^{(\text{input CT}-\text{bound CT})}$. The sequences of primers used in the qChIP experiments were shown (Table S3).

Lentivirus shRNA experiments and plasmid constructions

Lentivirus containing short hairpin RNAs (shRNAs) expressed in a lentiviral vector (pLKO.1-puro) were generated in 293T cells as previously described [25]. The sequence and clonal names of plasmid pLKO-scrambled or other pLKO plasmids knocking down *USP7* and the knockdown procedures were described [25] (Table S4).

The constructions of plasmids (pCl-neo Flag USP7, Myc-Flag-HNF4a, Myc-Flag-CEBPa, and Myc-Flag-GYS2) were performed by inserting each full-length cDNA into the pCl-neo or pCMV6 plasmid (Table S5). In the reconstitution experiments, we used QuikChange II Site-directed mutagenesis kit (Agilent) to generate K443R mutation of *USP7* in the pCl-neo Flag USP7 plasmid and transiently transfected pCl-neo vector, pCl-neo Flag USP7 ($USP7^{WT}$) or pCl-neo Flag $USP7^{K443R}$ expression vector inside *USP7*-knockdowned NeHepLxHT cells by using PolyJet™ In Vitro DNA Transfection Reagent.

Immunohistochemistry (IHC) and scoring

Four μm thick sections of all tissue were cut from the paraffin-embedded specimens for H&E and IHC staining. The samples were fixed in 4% paraformaldehyde solution for 24 h. The endogenous peroxidase activity was eliminated with 3% hydrogen peroxide and then incubated with 1% bovine serum albumin and 5% normal goat serum for the blocking step. After reacting with a biotinylated secondary antibody for 1.5 h, antigen–antibody reactions were visualized using streptavidin–horseradish peroxidase conjugate (DAKO LSAB kit; DAKO, Los Angeles, CA, USA), with 3-amino-9-ethylcarbazole as the chromogen. All slides were counterstained with hematoxylin. The antibodies used in IHC were listed (Table S1).

Mouse biochemistry profile, X-ray and CT scan of bones/muscles, and measurement of muscle weight

The biochemistry profile of different mouse strains, including wild-type, $Usp7^{WT/K444R}$, and $Usp7^{K444R/K444R}$ (three mice per group), were analyzed by TMC (Taiwan Mouse Clinic, Academia Sinica, Taiwan) and serum creatinine level was analyzed by a Creatinine Colorimetric/Fluorometric Assay Kit (cat. K625, Biovision, Milpitas, CA, USA). X-ray and CT (Computed Tomography) scan were authorized and performed by Center for Advanced Molecular Imaging and Translation, Chang Gung Medical Foundation, to measure the skeleton of tibia and fibula, and the muscles of hind limb, forearm, and Pectoralis. The muscle weight of hind limb, forearm, and Pectoralis were freshly dissected and immediately weighed on a balance with a readability of 0.1 mg. Relative muscle wet weight ratio represented the muscle wet weight normalized to the body weight of each mouse.

Statistical analysis

The independent Student's *t*-test was used to compare the continuous variables. The Kaplan–Meier estimate was used for survival analysis, and the log-rank test was used to compare the difference. The level of statistical significance was set at 0.05 for all tests.

Results

Decreased body weight and liver weight in the Usp7^{K444R} *mutant mice*

To test the physiological function of K63-polyubiquitinated Usp7, the polyubiquitination site (K444) of *Usp7* was mutated to arginine (R) by a traditional knock-in approach, and confirmed by sequencing (Fig. 1A and B). Compared to wild-type mice, *Usp7*^{K444R} mice showed a lower body weight and a smaller body size (Fig. 1A, C). Dissection of the mice revealed that the *Usp7*^{K444R} mice exhibited smaller livers and a lower liver weight than the wild-type mice (Fig. 1D and E), although H&E staining did not show morphologic abnormalities (Fig. 1F). The measurement and H&E staining of other organs, including heart, lung, stomach, spleen, intestine, bladder, and testis, did not reveal any difference in weight or histology between *Usp7*^{K444R} and wild-type mice (Supplementary Fig. 1). However, whole-body X-ray and CT scan of the *Usp7*^{K444R} mice showed decreased tibia and ulna length compared to that of the wild-type mice (Supplementary Fig. 2A). Imaging of muscle mass revealed decreased hind limb and forearm size in the *Usp7*^{K444R} mice, which was confirmed by the measurement of wet weight (Supplementary Fig. 2B). In the *Usp7*^{K444R} mice, the mRNA and protein levels of Usp7^{K444R} were not different from those of the wild-type mice (Supplementary Fig. 2C), indicating that the observed phenotypes were caused by Usp7^{K444R}. These results indicate that abolishing the K63-polyubiquitination of Usp7 causes small body size, lower liver weight, and abnormal skeletal and muscle phenotypes in *Usp7*^{K444R} mice.

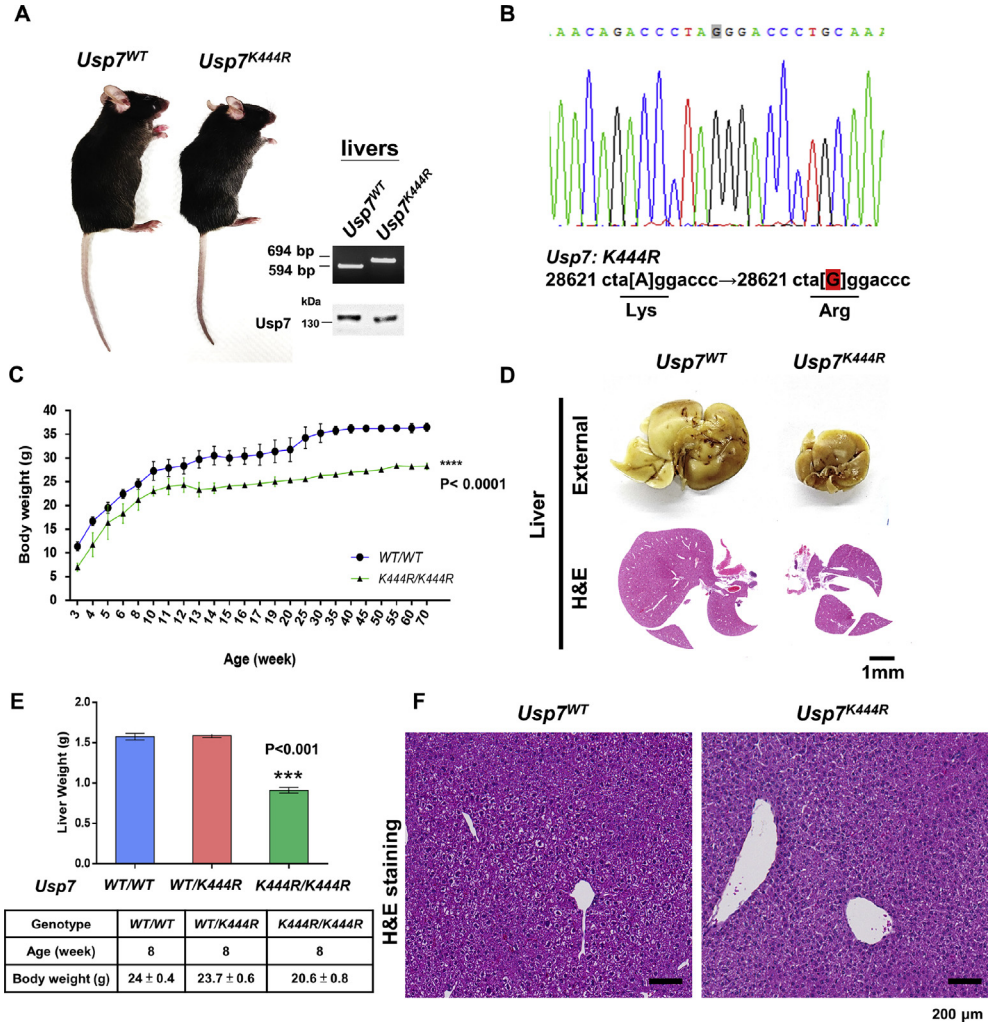

Genotype	WT/WT	WT/K444R	K444R/K444R
Age (week)	8	8	8
Body weight (g)	24 ± 0.4	23.7 ± 0.6	20.6 ± 0.8

Fig. 1 *Usp7*^{K444R} mutant mice had decreased body weight and liver size. (A) The gross appearance of wild type vs. *Usp7*^{K444R} mutant mice and confirmation of the point mutation by size difference using PCR analysis. Western blot analysis using extracts from liver showed the similar size of wild type vs. mutant Usp7. (B) Sequencing results confirmed the point mutation (K to R at the amino acid 444 position) in the homozygous point mutation mice. (C) Decreased body weight of the *Usp7*^{K444R} mutant mice was observed. Twenty mice were used for each group. (D) Decreased liver size in the *Usp7*^{K444R} mutant mice. (E) Decreased liver weight in the *Usp7*^{K444R} mutant mice. The measurement of liver weight at 8-week of age were shown. There is a statistical significance between wild-type and *Usp7*^{K444R} mutant mice ($p < 0.001$). Six mice were used for each group. (F) Normal liver histology in the *Usp7*^{K444R} mutant mice. Three mice were used for each group. Scale bars represented 200 μm.

Blood biochemistry profile of Usp7^{K444R} *mutant mice*

The blood biochemistry profile of the *Usp7*^{K444R} mice showed that LDL-C levels were decreased and HDL-C and serum creatinine levels were increased in the *Usp7*^{K444R} mice compared with those of wild-type mice (Supplementary Fig. 2D and E). The measurement of liver enzymes also showed the increased Got levels in the *Usp7*^{K444R} mice (Supplementary Fig. 2F). These results indicate that serological abnormalities exist in these mice.

Impaired mTorc2/Akt1 pathway in the Usp7^{K444R} *mutant mice*

We speculated that the smaller liver size and lower liver weight in the *Usp7*^{K444R} mice might be due to defective hepatocyte proliferation. Liver growth and development are known to be regulated by the mTORC2/AKT1 pathway [29]. We examined the phosphorylation levels of Mtor and Akt1 by Western blot analysis and found that, compared with wild-type, the levels of both p-Mtor (S2448) and p-Akt1 (S473) were significantly decreased in the *Usp7*^{K444R} mouse liver, whereas the levels of p-Akt1 (T308) were unchanged (Fig. 2A and Supplementary Fig. 3A). The phosphorylation level of Rps6kβ1, a downstream target of mTorc2, was also decreased (Fig. 2A). The levels of other proteins regulating the Pi3k/Akt1 pathway, including the Pi3kα, Pi3kβ, and Pi3kγ subunits, Pi3 kinase p85, and Pten, were not changed (Supplementary Fig. 3A). Since the mTORC2 complex activates AKT1 [29–32], we examined the levels of Mtor, Rictor, Mapkap1, Mlst8 and Prr5/Prr5l. We discovered that the protein levels of Prr5l, but not those of Prr5, Mapkap1, Rictor, or Mlst8, were decreased in the *Usp7*^{K444R} mouse liver (Fig. 2B). Knocking down *USP7* in a normal human liver cell line (NeHepLxHT) decreased the levels of phosphorylated MTOR(S2448) and AKT1(S473) as well as the level of PRR5L (Supplementary Fig. 3B and C). To test whether PRR5L is a substrate of USP7, coimmunoprecipitation experiments showed that USP7 interacted with PRR5L in the NeHepLxHT cell line (Fig. 2C), indicating that PRR5L is a putative USP7 substrate. With 293T cells overexpressing Myc-tagged PRR5L and Flag-tagged USP7, coimmunoprecipitation experiments using anti-USP7 or anti-Myc-Tag antibodies showed an interaction between USP7 and PRR5L (Fig. 2D). After verifying the interaction between these two proteins, deubiquitination assays by incubating purified USP7 (wild type vs. K443R mutant) and K48-polyubiquitinated PRR5L showed that only wild-type USP7 was capable of deubiquitinating K48-polyubiquitinated PRR5L (Fig. 2E). The levels of K63-polyubiquitinated PRR5L were not detectable (Fig. 2E). In the NeHepLxHT cell line, after knocking down endogenous *USP7*, reconstitution of USP7 with a vector containing wild-type *USP7* restored the PRR5L level, whereas reconstitution with a vector containing *USP7*^{K443R} did not restore the PRR5L level (Fig. 2F), supporting the conclusion that PRR5L is a USP7 substrate. Compared to its expression in wild-type, the level of Yap1 that regulates cell growth and is regulated by Usp7 was also decreased in *Usp7*^{K444R} mouse liver [34], whereas the mRNA levels of *Yap1* were not changed (Supplementary Fig. 4A and B). The reconstitution experiments showed that YAP1 was regulated by USP7 in NeHepLxHT cells (Supplementary Fig. 4C). Since YAP1 has been shown to be regulated by the FGF15 signaling [35,36], we further tested this pathway. Western blot analysis showed that Fgf15 levels were decreased and Mst1/2 levels were increased in *Usp7*^{K444R} mouse liver (Supplementary Fig. 4A). The Yap1/p-Yap1 levels were decreased due to the increased Mst1 levels that caused the repression of Yap1 (Supplementary Fig. 4A). The reconstitution experiments showed that FGF15 and YAP1 levels were rescued by wild type USP7 in NeHepLxHT cells, whereas MST1/2 levels were decreased by wild type USP7 (Supplementary Fig. 4C). The levels of K63-polyubiquitnated Usp7 were decreased in the liver of the *Usp7*^{K444R} mutant mice compared with those in the liver of the wild-type mice (Supplementary Fig. 4D). Finally, immunohistochemistry staining showed that the levels of p-Akt1 (S473), p-Mtor (S2448), and Prr5l were decreased in *Usp7*^{K444R} mouse liver compared with those in the wild-type liver (Fig. 2G), but there was no difference in the staining of Prr5, Rictor, or p-Akt1 (T308) (Supplementary Fig. 4E).

Liver glycogen storage defect in the Usp7^{K444R} *mutant mice*

As one of the major functions of the liver is glycogen storage, we performed periodic acid-schiff (PAS) staining to compare the liver glycogen levels between *Usp7*^{K444R} and wild-type mice. Glycogen staining was greatly decreased in the livers of the *Usp7*^{K444R} mice (Fig. 3A). Glycogen synthase 2 (Gys2) is the rate limiting enzyme of glycogen synthesis in the liver [37]. To determine if Gys2 is involved in the glycogen storage defect of *Usp7*^{K444R} mice, immunohistochemistry staining and Western blotting were performed; both methods showed significantly lower Gys2 protein levels in the liver of the *Usp7*^{K444R} mice compared with those in the livers of the wild-type mice (Fig. 3B and C). We further measured the mRNA levels of *Gys2* and found that its levels were significantly lower in the *Usp7*^{K444R} mice (Fig. 3D). To test the ability of Usp7 to regulate Gys2 expression, we knocked down USP7 expression in NeHepLxHT cells followed by re-expression of either USP7 or USP7^{K443R}. The results showed that re-expression of wild-type USP7 restored the GYS2 protein levels, whereas re-expression of USP7^{K443R} did not (Fig. 3E). As demonstrated previously, USP7^{K443R} greatly reduces its ability to deubiquitinate and stabilize its substrate proteins [25]. To determine whether GYS2 is a substrate of USP7, we performed a protein turnover assay with *USP7*-knockdown NeHepLxHT cells re-expressing either USP7 or USP7^{K443R} and treated them with cycloheximide (CHX) at different time points to inhibit protein synthesis. If GYS2 protein stability is regulated by wild-type but not mutant USP7, then there will be a difference in the half-life of GYS2 protein between these two conditions. However, there was no difference in GYS2 protein turnover between the two conditions (Supplementary Fig. 4F), indicating that USP7 does not regulate GYS2 protein degradation or half-life. The above results suggest

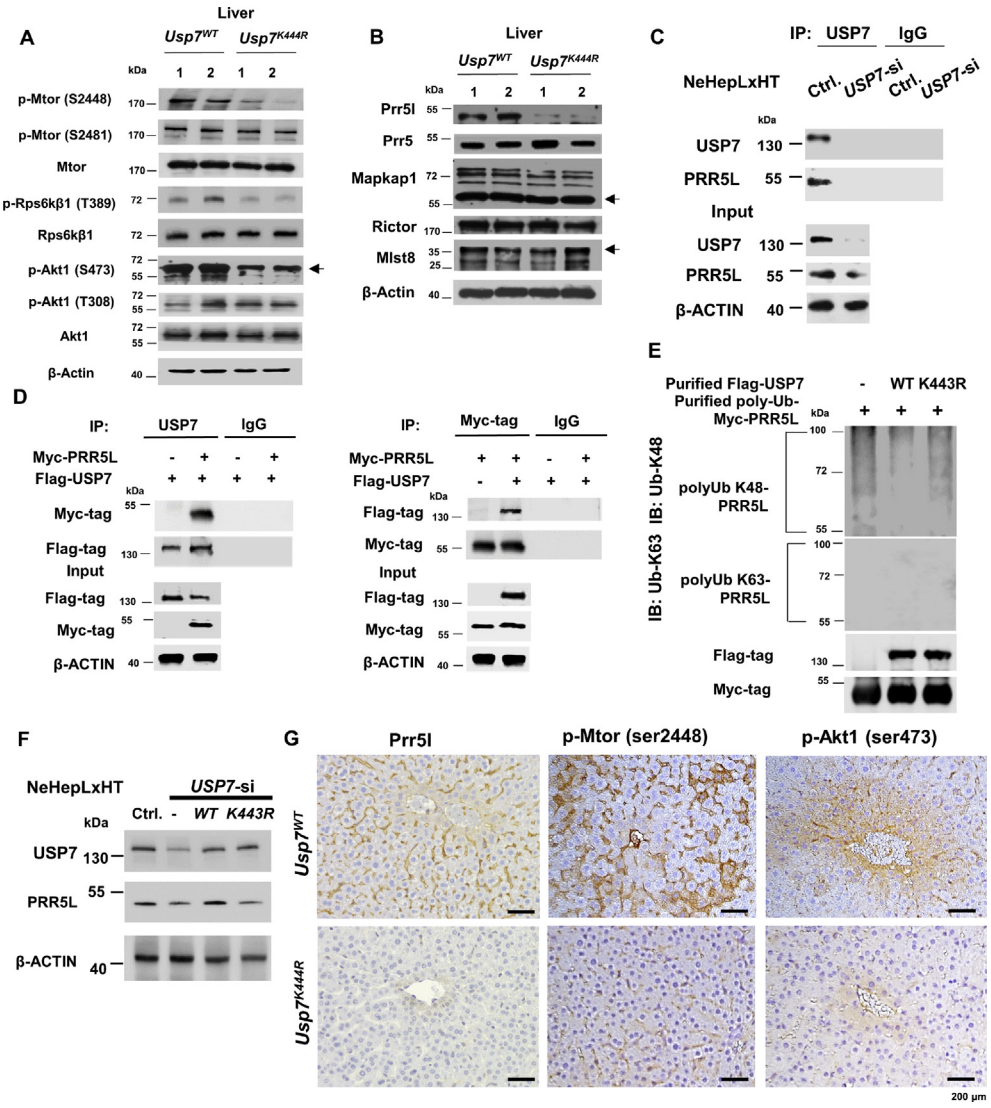

Fig. 2 Impaired Mtor/Akt1 activity in the *Usp7*^{K444R} mutant mice. (A) *Usp7*^{K444R} mutant mice had decreased phosphorylation levels of Mtor (Ser2448) and Akt1 (Ser473) by Western blot analysis of liver extracts. (B) Decreased Prr5l level in the liver extracts from the *Usp7*^{K444R} mutant mice. Labeling of 1 and 2 in (A, B) represented one mouse of each experiment. Six mice were used for each group in (A, B). (C) Coimmunoprecipitation experiments showed an interaction between USP7 and PRR5L and knocking down *USP7* decreased the PRR5L level and the interaction between USP7 and PRR5L in NeHepLxHT cells. (D) Coimmunoprecipitation experiments showed an interaction between USP7 and PRR5L where both proteins were overexpressed in 293T cells followed by antibody pull down using either anti-USP7 or anti-Myc antibodies. (E) Deubiquitination assays showed a decreased ability of USP7^{K443R} to deubiquitinate K48-polyubiquitinated PRR5L. The levels of K63-polyubiquitinated PRR5L served as a control. (F) Knocking down *USP7* in a NeHepLxHT cell line followed by reconstitution with a wild-type USP7 restored the PRR5L level, whereas reconstitution with a USP7^{K443R} mutant did not rescue the PRR5L level. (G) Immunohistochemistry staining showed the decreased levels of Prr5l, p-Mtor (Ser2448) and p-Akt1 (Ser473) in the liver of the *Usp7*^{K444R} mutant mice. Six mice were used for each group. Scale bars represented 200 μm.

that the regulation of *Gys2* by Usp7 in *Usp7*^{K444R} mutant mice occurs at the transcriptional level.

Regulation of Hnf4α and Cebpα by K63-polyubiquitinated Usp7

Since *Gys2* may be regulated by Usp7 at the transcriptional level, we tested whether Hnf4α and Cebpα, two major transcription factors regulating *Gys2* gene transcription, play a role in this process [38–40]. Western blot analysis showed that the protein levels of Hnf4α and Cebpα were remarkably lower in the *Usp7*^{K444R} mice than in the wild-type mice (Fig. 4A), whereas immunohistochemistry staining showed no difference in the protein levels of Hnf1α (Supplementary Fig. 5A). Furthermore, the mRNA levels of both *Hnf4a* and *Cebpa* were significantly decreased in the *Usp7*^{K444R} mice (Fig. 4B). This finding was confirmed in NeHepLxHT cells, in which reconstitution of the USP7^{K443R} did not restore the decreased levels of HNF4α and CEBPα (Fig. 4C). In addition, the half-lives of HNF4α and CEBPα were significantly longer in *USP7*-

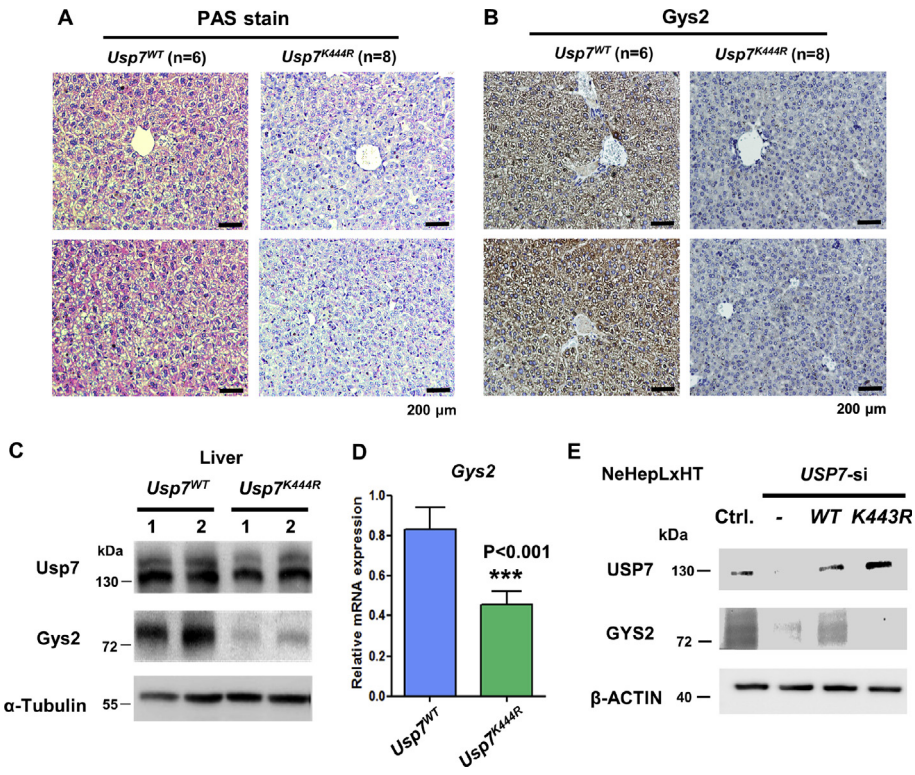

Fig. 3 Glycogen storage defect in the liver of the *Usp7*^{K444R} mutant mice. (A) Decreased PAS staining in the liver of the *Usp7*^{K444R} mutant mice. (B) Decreased Gys2 staining in the *Usp7*^{K444R} mutant mice by immunohistochemistry staining. Six mice were used for wild-type mice and eight mice were used for *Usp7*^{K444R} mutant mice. Labeling of #1 and #2 represented one mouse of each experiment. Scale bars represented 200 μm in (A, B). (C) Decreased Gys2 protein level from the liver extracts of the *Usp7*^{K444R} mutant mice by Western blot analysis. Labeling of 1 and 2 represented one mouse of each experiment. (D) Decreased *Gys2* mRNA levels in the liver of the *Usp7*^{K444R} mutant mice. Six mice were used for each group. (E) Restoration of the GYS2 protein level by a wild-type USP7, but not a USP7^{K443R} mutant, in the NeHepLxHT cells undergoing *USP7* knockdown.

knockdown NeHepLxHT cells reconstituted with USP7 than in those reconstituted with USP7^{K443R} (Supplementary Fig. 5B and C). These results indicate that both HNF4α and CEBPα are USP7 substrates. Immunohistochemistry staining also confirmed the decreased levels of Hnf4α and Cebpα in the *Usp7*^{K444R} mice compared with those in the wild-type mice (Fig. 4D). Finally, immunohistochemistry staining of other liver development markers potentially regulated by Hnf4α, including Pecam1, Tjp1, and E-cadherin [41–43], showed that their protein levels were decreased in the *Usp7*^{K444R} mutant livers (Supplementary Fig. 6A), supporting this regulation.

To demonstrate the interaction between USP7 and HNF4α, co-immunoprecipitation experiments with two different cell lines showed an interaction between USP7 and HNF4α (Supplementary Fig. 6B), suggesting that HNF4α is a substrate of USP7. The USP7^{K443R} mutant could not rescue the protein levels of HNF4α in the *USP7*-knockdown NeHepLxHT cells (Supplementary Fig. 6C). Since USP7 also serves as a scaffold to anchor the HIF1α transcription complex to regulate the transcription of certain HIF1α target genes [25], we investigated two and five hypoxia response elements (HREs) in their promoter regions of *Hnf4a* and *Cebpa* genes, respectively (Fig. 4E and F). We performed a qChIP assay to determine whether Hif1α directly binds to the promoter region of these genes. The binding of Hif1α to the HREs located in the *Hnf4a* and *Cebpa* promoters in the *Usp7*^{K444R} mutant mice was significantly reduced compared with that in the wild-type mice (Fig. 4E and F). These results indicate that Hnf4α and Cebpα may be regulated at both the translational and transcriptional levels by K63-polyubiquitinated Usp7.

Polycystic kidney disease in the Usp7^{K444R} *mutant mice*

When we further examined organ defects, we discovered that the *Usp7*^{K444R} mice exhibited polycystic kidneys (Fig. 5A). Histology confirmed the existence of polycystic kidneys in these mice (Fig. 5B). The mice developed polycystic kidneys as early as four weeks of age, and by seven months of age, all the mice showed polycystic kidneys (Fig. 5C). The appearance of kidney cysts at different time points is shown (Supplementary Fig. 7A). Using Western blot and immunohistochemistry staining, we screened for putative regulators crucial for polycystic kidney formation and discovered that the protein levels of Pkd2 and Pkhd1, whose mutation causes polycystic kidney disease [44–47], were decreased in the *Usp7*^{K444R} kidneys compared with the wild-type kidneys (Fig. 5D and E). In addition, the protein level of Hnf1β, the upstream regulator of *Pkd2* and *Pkhd1* [47], was also decreased in the mutant, as

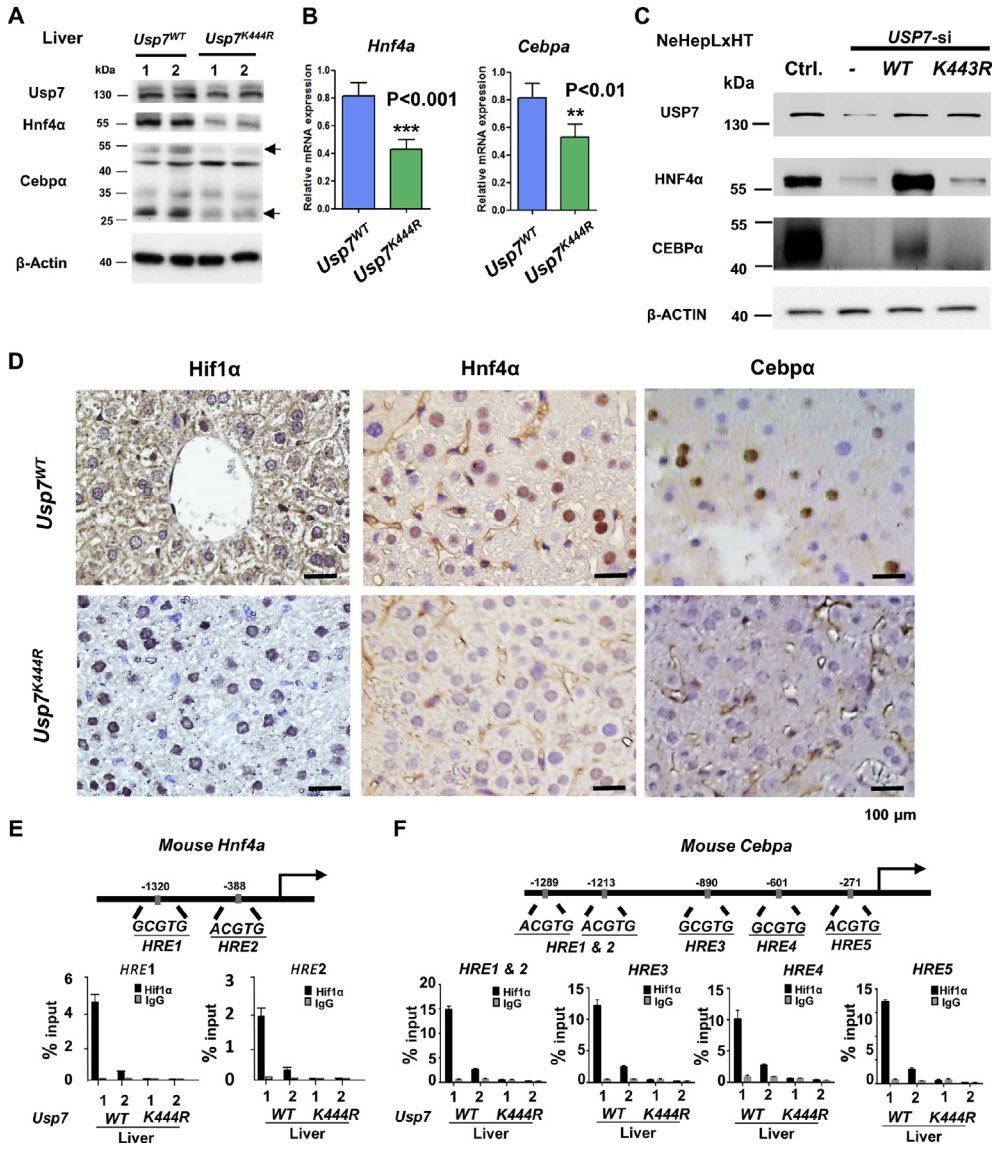

Fig. 4 Regulation of Gys2 expression by Hnf4α and Cebpα in mouse liver. (A) Western blot analysis showed decreased Hnf4α and Cebpα levels in the liver extracts of *Usp7*^{K444R} mutant mice. Labeling of 1 and 2 represented one mouse of each experiment. (B) Decreased *Hnf4a* and *Cebpa* mRNA levels in the liver of the *Usp7*^{K444R} mutant mice. Six mice were used for each group. (C) Restoration of the HNF4α and CEBPα protein levels by a wild-type USP7, but not a USP7^{K443R} mutant, in the NeHepLxHT cells undergoing *USP7* knockdown. (D) Immunohistochemistry staining showed decreased Hnf4α and Cebpα levels in the liver of the *Usp7*^{K444R} mutant mice. Scale bars represented 100 μm. (E, F) qChIP assays showed the binding of Hif1a to the HREs located in the promoters of the *Hnf4a* and *Cebpa* genes in the wild-type mice, but not in the *Usp7*^{K444R} mutant mice. Blue colored symbols represented wild-type; green colored symbols represented mutant in (E, F). Six mice were used for each group in (A, B, D-F).

shown by Western blot analysis and immunohistochemistry staining (Fig. 5D, F). Consistent with these results, the mRNA levels of *Hnf1b*, *Pkd2*, and *Pkhd1* were decreased in the *Usp7*^{K444R} mice compared with those in the wild-type mice (Supplementary Fig. 7B). The levels of K63-polyubiquitnated Usp7 were also decreased in the kidney of the *Usp7*^{K444R} mice (Supplementary Fig. 7C). In contrast, immunohistochemistry staining and mRNA analysis of Pkd1 showed no difference in Pkd1 expression between wild type and mutant mouse strains (Supplementary Fig. 7D). To ascertain whether the *Hnf1b* promoter is regulated by K63-polyubiquitinated Usp7, HREs were identified in the promoter of the *Hnf1b* gene. qChIP assays showed decreased binding of Hif1α to the HREs of the *Hnf1b* gene in the *Usp7*^{K444R} mice compared with that in the wild-type mice (Fig. 5G), supporting the conclusion that K63-polyubiquitinated Usp7 serves as a scaffold to enhance Hif1α-induced gene transcription of *Hnf1b*, similar to what was observed in the promoters of the *Hnf4a* and *Cebpa* genes (Fig. 4E and F). Finally, the *Usp7*^{K444R} mice strain had a decreased life span compared with the wild-type mice (Fig. 5H), suggesting that the organ defects observed in this mouse may influence life span.

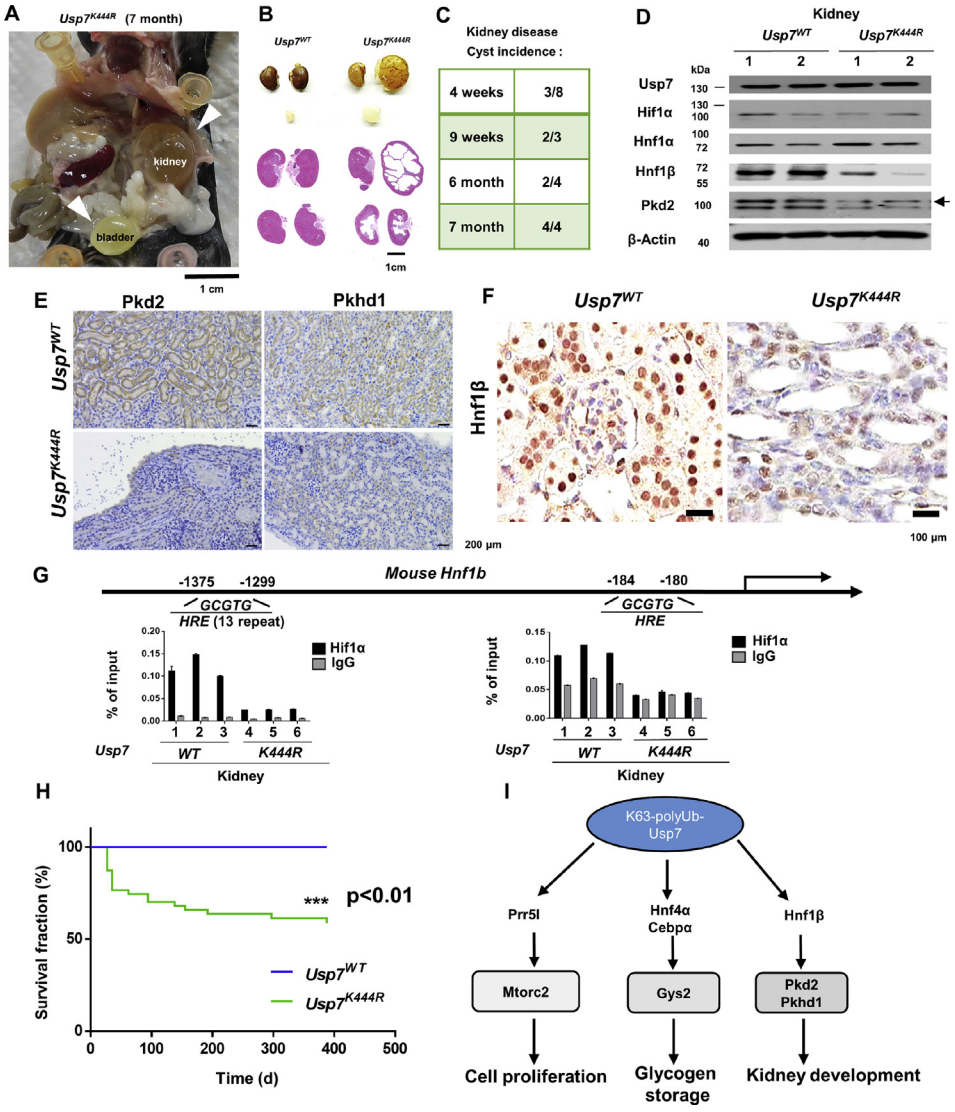

Fig. 5 Presentation of the polycystic kidney phenotype and its signaling pathway in the *Usp7*^{K444R} mutant mice together with a model to summarize all the signaling pathways causing the organ defect phenotypes observed in the *Usp7*^{K444R} mutant mice. (A) Gross anatomy of the *Usp7*^{K444R} mutant mouse kidneys showed polycystic kidney disease (PKD). (B) Gross appearance of kidneys and their histology showed the phenotype of polycystic kidneys in the *Usp7*^{K444R} mutant mice (at the age of 9 weeks and 25 weeks). The two kidneys shown were from the same mouse, suggesting asymmetric cystogenesis for the mouse at the age of 9 weeks. (C) By 7 months of age, all *Usp7*^{K444R} mutant mice exhibited polycystic kidneys. (D) Decreased Hnf1β and Pkd2 protein levels from the kidney extracts in the *Usp7*^{K444R} mutant mice. Labeling of 1 and 2 represented one mouse of each experiment. (E) Immunohistochemistry showed decreased Pkd2 and Pkhd1 staining in the kidneys of the *Usp7*^{K444R} mutant mice. Scale bars represented 200 μm. (F) Immunohistochemistry showed decreased Hnf1b staining in the kidneys of the *Usp7*^{K444R} mutant mice. Six mice were used for each group in (D–F). Scale bars represented 100 μm. (G) qChIP assays showed decreased binding of Hif1α to the promoter of *Hnf1b* gene in the *Usp7*^{K444R} mutant mice compared to that in the wild-type mice. Blue colored symbols represented wild-type; green colored symbols represented mutant. Nine mice were used for each group. (H) Decreased life span in the *Usp7*^{K444R} mutant mice compared to that in the wild-type mice. (I) A model to summarize all the signaling pathways that regulate liver size, glycogen storage, kidney development through the analysis of the phenotypes of the *Usp7*^{K444R} mutant mice.

Discussion

K63-linked polyubiquitination controls the activity of many important signal transduction pathways [1–11]. However, the *in vivo* effects of K63-polyubiquitinated proteins have rarely been assessed due to the requirement to generate point mutants of specific proteins by knock-in approach. USP7 is a deubiquitinase for many important proteins [16–25], and its *in vivo* phenotypes have been difficult to analyze due to the phenotypes of whole body or neuron-specific *Usp7*-null mouse strains not yielding logical results [26,27]. In this report, we show that a K63 polyubiquitination-defective Usp7 point mutant mouse strain demonstrates prominent phenotypes,

including decreased liver and muscle weight, smaller tibia/fibula length, deficient liver glycogen storage, and polycystic kidneys. The hypomorphic nature of K63 polyubiquitination-defective Usp7 mutant mice allows their phenotypes to be observed and analyzed.

Our previous results showed that K63-linked polyubiquitination of USP7 has two functions: enhancing the deubiquitinase activity of USP7 and enabling it to serve as a scaffold to coordinate HIF1α-induced gene transcription [25]. In this report, our results show that the organ defects are mediated either through the impaired Usp7 deubiquitinase activity (Prr5l, Hnf4α, Cebpα as Usp7 substrates), or impaired Usp7 scaffolding ability during Hif1α-induced gene transcription (*Hnf4a*, *Cebpa*, and *Hnf1b* genes). Therefore, by observing the phenotypes of $Usp7^{K444R}$ mice, the mechanistic roles of K63-polyubiquitinated Usp7 can be deduced, and the biological functions of USP7 can be further delineated.

Regarding the decrease in liver weight and size, mTORC2 complex has been shown to regulate cell proliferation [29]. Recent results showed that mTORC2 complex also regulates cell size and growth through different mechanisms, including the activation of mTORC1 and c-Myc in B cell growth, regulation of Purkinje cell size, and control of ceramide signaling in yeast cell size and growth [48–50]. Our results showed that Prr5l contributes to the phosphorylation of Akt1(S-473) and regulates cell proliferation, supporting the conclusion that mTORC2 signaling controls liver growth and size. The decreased level of Yap1 in mutant mice is another factor that may contribute to their decreased weight and size [33,34]. Furthermore, the FGF15-MST1/2-YAP1 axis is also involved in regulating liver size from examining this signaling pathway in $Usp7^{K444R}$ mutant mice (Supplementary Fig. 4A, C). How USP7 regulates this pathway remains to be determined. In terms of organ defects, our results suggest that the molecular mechanisms of known human diseases (e.g., glycogen storage defect) are not mediated by gene mutations alone (e.g., mutation of *GYS2* in glycogen storage disease type 0) [37]. Our results indicate that the $Usp7^{K444R}$ mutant protein contributed to a disease similar to glycogen storage disease type 0. Regarding PKD, the downregulation of *Pkd2* and *Pkhd1* through K63 polyubiquitination-defective Usp7 that leads to decreased *Hnf1b* level also led to the polycystic kidney phenotype, consistent with prior observations [33,34]. Mutations that cause K63 polyubiquitination-defective USP7 may lead to human polycystic kidney disease. For the variable PKD phenotypes shown (Fig. 5B), "variable expressivity" has been observed in chronic kidney disease [51] and may provide the explanation.

Conclusions

Our results suggest possible novel molecular mechanisms (i.e. K63-linked polyubiquitination of USP7) for these known human genetic diseases. A summary of all signaling pathways identified in this report is shown (Fig. 5I). Furthermore, the important biological functions of K63-linked polyubiquitinated proteins could be more carefully assessed using an *in vivo* knock-in approach to express a protein with a point mutation in its K63 polyubiquitination site.

Ethics approval

Handling of the animals was approved by the Internal Animal Usage Committee of the Chang Gung Memorial Hospital at Linkou.

Funding

This work was supported in part to K.J.W. by Ministry of Science and Technology Summit and Frontier grants (MOST 108-2321-B-182A-005, MOST 109-2326-B-182A-002; MOST 110-2326-B-182A-004), Chang Gung Memorial Hospital (OMRPG3I0012, NMRPG3J6192, CORPG3J0232, NMRPG3J0672, CORPG3J0261, CORPG3J062, NMRPG3J0673, NMRPG3J6193, CORPG3J0233, OMRPG3I0013) and to H.T.W. (MOST 108-2314-B-371-002).

Consent for publication

Not applicable.

Availability of data and material

The data and material will be available from the corresponding author upon reasonable request.

Code availability

Not applicable.

Conflicts of interest

The authors declare that they have no conflicts of interest.

Acknowledgments

We thank the Center for Advanced Molecular Imaging and Translation, Chang Gung Medical Foundation for performing CT scan of mice.

Appendix A. Supplementary data

Supplementary data to this article can be found online at https://doi.org/10.1016/j.bj.2022.02.002.

REFERENCES

[1] Chen ZJ, Sun LJ. Nonproteolytic functions of ubiquitin in cell signaling. Mol Cell 2009;33(3):275–86.

[2] Yang WL, Zhang X, Lin HK. Emerging role of Lys-63 ubiquitination in protein kinase and phosphatase activation and cancer development. Oncogene 2010;29(32):4493–503.
[3] Yan K, Ponnusamy M, Xin Y, Wang Q, Li P, Wang K. The role of K63-linked polyubiquitination in cardiac hypertrophy. J Cell Mol Med 2018;22(10):4558–67.
[4] Chen J, Chen ZJ. Regulation of NF-κB by ubiquitination. Curr Opin Immunol 2013;25(1):4–12.
[5] Chen ZJ. Ubiquitination in signaling to and activation of IKK. Immunol Rev 2012;246(1):95–106.
[6] Harhaj EW, Dixit VM. Regulation of NF-κB by deubiquitinases. Immunol Rev 2012;246(1):107–24.
[7] Yazlovitskaya EM, Tseng HY, Viquez O, Tu T, Mernaugh G, McKee KK, et al. Integrin α3β1 regulates kidney collecting duct development via TRAF6-dependent K63-linked polyubiquitination of Akt. Mol Biol Cell 2015;26(10):1857–74.
[8] Martinez-Forero I, Rouzaut A, Palazon A, Dubrot J, Melero I. Lysine 63 polyubiquitination in immunotherapy and in cancer-promoting inflammation. Clin Cancer Res 2009;15(22):6751–7.
[9] Wang T, Wang J. K63-linked polyubiquitination of IRF1: an essential step in the IL-1 signaling cascade. Cell Mol Immunol 2014;11(5):407–9.
[10] Okamoto M, Kouwaki T, Fukushima Y, Oshiumi H. Regulation of RIG-I activation by K63-linked polyubiquitination. Front Immunol 2017;8:1942.
[11] Atanassov BS, Koutelou E, Dent SY. The role of deubiquitinating enzymes in chromatin regulation. FEBS Lett 2011;585(13):2016–23.
[12] Leznicki P, Kulathu Y. Mechanisms of regulation and diversification of deubiquitylating enzyme function. J Cell Sci 2017;130(12):1997–2006.
[13] Hussain S, Zhang Y, Galardy PJ. DUBs and cancer: the role of deubiquitinating enzymes as oncogenes, non-oncogenes and tumor suppressors. Cell Cycle 2009;8(11):1688–97.
[14] Komander D, Clague MJ, Urbé S. Breaking the chains: structure and function of the deubiquitinases. Nat Rev Mol Cell Biol 2009;10(8):550–63.
[15] Reyes-Turcu FE, Ventii KH, Wilkinson KD. Regulation and cellular roles of ubiquitin-specific deubiquitinating enzymes. Annu Rev Biochem 2009;78:363–97.
[16] Bhattacharya S, Chakraborty D, Basu M, Ghosh MK. Emerging insights into HAUSP (USP7) in physiology, cancer and other diseases. Signal Transduct Target Ther 2018;3:17.
[17] Rawat R, Starczynowski DT, Ntziachristos P. Nuclear deubiquitination in the spotlight: the multifaceted nature of USP7 biology in disease. Curr Opin Cell Biol 2019;58:85–94.
[18] Nicholson B, Suresh Kumar KG. The multifaceted roles of USP7: new therapeutic opportunities. Cell Biochem Biophys 2011;60((1-2)v):61–8.
[19] Colleran A, Collins PE, O'Carroll C, Ahmed A, Mao X, McManus B, et al. Deubiquitination of NF-κB by ubiquitin-specific protease-7 promotes transcription. Proc Natl Acad Sci U S A 2013;110(2):618–23.
[20] Li M, Chen D, Shiloh A, Luo J, Nikolaev AY, Qin J, et al. Deubiquitination of p53 by HAUSP is an important pathway for p53 stabilization. Nature 2002;416(6881):648–53.
[21] Cummins JM, Vogelstein B. HAUSP is required for p53 destabilization. Cell Cycle 2004;3(6):689–92.
[22] Meulmeester E, Maurice MM, Boutell C, Teunisse AF, Ovaa H, Abraham TE, et al. Loss of HAUSP-mediated deubiquitination contributes to DNA damage-induced destabilization of Hdmx and Hdm2 [published correction appears in Mol Cell 2005;19:143–4]. Mol Cell 2005;18(5):565–76.
[23] Huang Z, Wu Q, Guryanova OA, Cheng L, Shou W, Rich JN, et al. Deubiquitylase HAUSP stabilizes REST and promotes maintenance of neural progenitor cells. Nat Cell Biol 2011;13(2):142–52.
[24] Song MS, Salmena L, Carracedo A, Egia A, Lo-Coco F, Teruya-Feldstein J, et al. The deubiquitinylation and localization of PTEN are regulated by a HAUSP-PML network. Nature 2008;455(7214):813–7.
[25] Wu HT, Kuo YC, Hung JJ, Huang CH, Chen WY, Chou TY, et al. K63-polyubiquitinated HAUSP deubiquitinates HIF-1α and dictates H3K56 acetylation promoting hypoxia-induced tumour progression. Nat Commun 2016;7:13644.
[26] Kon N, Kobayashi Y, Li M, Brooks CL, Ludwig T, Gu W. Inactivation of HAUSP in vivo modulates p53 function. Oncogene 2010;29(9):1270–9.
[27] Kon N, Zhong J, Kobayashi Y, Li M, Szabolcs M, Ludwig T, et al. Roles of HAUSP-mediated p53 regulation in central nervous system development. Cell Death Differ 2011;18(8):1366–75.
[28] Ginzberg MB, Kafri R, Kirschner M. Cell biology. On being the right (cell) size. Science 2015;348(6236):1245075.
[29] Saxton RA, Sabatini DM. mTOR signaling in growth, metabolism, and disease [published correction appears in Cell 2017;169:361–71]. Cell 2017;168(6):960–76.
[30] Thedieck K, Polak P, Kim ML, Molle KD, Cohen A, Jenö P, et al. PRAS40 and PRR5-like protein are new mTOR interactors that regulate apoptosis. PLoS One 2007;2(11):e1217.
[31] Woo SY, Kim DH, Jun CB, Kim YM, Haar EV, Lee SI, et al. PRR5, a novel component of mTOR complex 2, regulates platelet-derived growth factor receptor beta expression and signaling. J Biol Chem 2007;282(35):25604–12.
[32] Pearce LR, Huang X, Boudeau J, Pawłowski R, Wullschleger S, Deak M, et al. Identification of Protor as a novel Rictor-binding component of mTOR complex-2. Biochem J 2007;405(3):513–22.
[33] Fu V, Plouffe SW, Guan KL. The Hippo pathway in organ development, homeostasis, and regeneration. Curr Opin Cell Biol 2017;49:99–107.
[34] Sun X, Ding Y, Zhan M, Li Y, Gao D, Wang G, et al. Usp7 regulates Hippo pathway through deubiquitinating the transcriptional coactivator Yorkie. Nat Commun 2019;10(1):411.
[35] Avruch J, Zhou D, Fitamant J, Bardeesy N. Mst1/2 signalling to Yap: gatekeeper for liver size and tumour development. Br J Cancer 2011;104(1):24–32.
[36] Ji S, Liu Q, Zhang S, Chen Q, Wang C, Zhang W, et al. FGF15 activates Hippo signaling to suppress bile acid metabolism and liver tumorigenesis. Dev Cell 2019;48(4).460–474.e9.
[37] Shin YS. Glycogen storage disease: clinical, biochemical, and molecular heterogeneity. Semin Pediatr Neurol 2006;13(2):115–20.
[38] Parviz F, Matullo C, Garrison WD, Savatski L, Adamson JW, Ning G, et al. Hepatocyte nuclear factor 4alpha controls the development of a hepatic epithelium and liver morphogenesis. Nat Genet 2003;34(3):292–6.
[39] Mandard S, Stienstra R, Escher P, Tan NS, Kim I, Gonzalez FJ, et al. Glycogen synthase 2 is a novel target gene of peroxisome proliferator-activated receptors. Cell Mol Life Sci 2007;64(9):1145–57.
[40] Qiao L, MacLean PS, You H, Schaack J, Shao J. Knocking down liver CCAAT/enhancer-binding protein alpha by adenovirus-transduced silent interfering ribonucleic acid improves hepatic gluconeogenesis and lipid homeostasis in db/db mice. Endocrinology 2006;147(6):3060–9.
[41] Battle MA, Konopka G, Parviz F, Gaggl AL, Yang C, Sladek FM, et al. Hepatocyte nuclear factor 4alpha orchestrates expression of cell adhesion proteins during the epithelial transformation of the developing liver. Proc Natl Acad Sci U S A 2006;103(22):8419–24.
[42] Santangelo L, Marchetti A, Cicchini C, Conigliaro A, Conti B, Mancone C, et al. The stable repression of mesenchymal program is required for hepatocyte identity: a novel role for hepatocyte nuclear factor 4α. Hepatology 2011;53(6):2063–74.

[43] Qu X, Lam E, Doughman YQ, Chen Y, Chou YT, Lam M, et al. Cited2, a coactivator of HNF4alpha, is essential for liver development. EMBO J 2007;26(21):4445–56.
[44] Bergmann C, Guay-Woodford LM, Harris PC, Horie S, Peters DJM, Torres VE. Polycystic kidney disease. Nat Rev Dis Prim 2018;4(1):50.
[45] Bergmann C. Genetics of autosomal recessive polycystic kidney disease and its differential diagnoses. Front Pediatr 2017;5:221.
[46] Foo JN, Xia Y. Polycystic kidney disease: new knowledge and future promises. Curr Opin Genet Dev 2019;56:69–75.
[47] Shao A, Chan SC, Igarashi P. Role of transcription factor hepatocyte nuclear factor-1β in polycystic kidney disease. Cell Signal 2020;71:109568.
[48] Thomanetz V, Angliker N, Cloëtta D, Lustenberger RM, Schweighauser M, Oliveri F, et al. Ablation of the mTORC2 component rictor in brain or Purkinje cells affects size and neuron morphology. J Cell Biol 2013;201(2):293–308.
[49] Li M, Lazorchak AS, Ouyang X, Zhang H, Liu H, Arojo OA, et al. Sin1/mTORC2 regulate B cell growth and metabolism by activating mTORC1 and Myc. Cell Mol Immunol 2019;16(9):757–69.
[50] Lucena R, Alcaide-Gavilán M, Schubert K, He M, Domnauer MG, Marquer C, et al. Cell size and growth rate are modulated by TORC2-dependent signals. Curr Biol 2018;28(2):196–210.e4.
[51] Groopman EE, Povysil G, Goldstein DB, Gharavi AG. Rare genetic causes of complex kidney and urological diseases. Nat Rev Nephrol 2020;16(11):641–56.